

Microstructure and Dielectric Properties of BaFe₁₂O₁₉ Hexaferrite Nanoparticles: Effect of Cobalt Addition and Calcination Temperature

H. Shehabi^a, M. Rekyb^b, R. Sayed Hassan^c and R. Awad^a

^a Department of Physics, Faculty of Science, Beirut Arab University, Beirut, Lebanon.

^b Department of Physics, Faculty of Science, Alexandria University, Alexandria, Egypt.

^b Department of Physics, Faculty of Science, Lebanese University, Beirut, Lebanon.

Doi : <https://doi.org/10.47011/13.3.4>

Received on: 08/08/2019;

Accepted on: 12/1/2020

Abstract: M-type Barium Hexaferrite (BaFe₁₂O₁₉) is a promising compound for technological applications because of its high permeability, high saturation magnetization and excellent dielectric properties. In this study, the microstructure and dielectric properties of Co_xBaFe₁₂O₁₉ Hexaferrite were investigated. The co-precipitation method was employed to prepare Co_xBaFe₁₂O₁₉ nanoparticles, with x = 0, 0.04, 0.06 and 0.1 wt. %, at two different calcination temperatures (900°C and 950°C). The microstructure of the samples was examined through X-ray powder diffraction (XRD) and transmission electron microscopy (TEM). The hexagonal structure of the prepared samples was confirmed from XRD results. TEM images reveal the formation of agglomerated nanoparticles with different size distribution. The dielectric properties of the samples were studied through HIOKI 3532-50 LCR-Hi TESTER as a function of frequency (100 kHz–3MHz) and temperature (25 °C–500°C). The effects of Co addition, frequency and temperature on the dielectric constants (ϵ' and ϵ''), loss tangent ($\tan \delta$) and ac conductivity (σ_{ac}) have been explained on the basis of hopping of electrons between Fe²⁺ and Fe³⁺ ions.

Keywords: BaFe₁₂O₁₉ Hexaferrite, Co-precipitation method, XRD, Dielectric properties.

Introduction

Hexaferrites form a wide category of ferromagnetic oxide materials that crystallize in complex hexagonal structure with space group P63/mmc [1]. There are six types of Hexaferrites, where the M-type Barium Hexaferrite “BaFe₁₂O₁₉” is the most important type both scientifically and technologically because of its various applications and amazing properties. Scientifically, BaFe₁₂O₁₉ has an excellent chemical stability and corrosion resistivity [2]. Technologically, BaFe₁₂O₁₉ can be used to manufacture permanent magnets and microwave absorbing devices. Also, it is used in

many applications in computer data storage, magneto-optic recording, disc drivers and video recorders [3, 4]. Ferromagnetic oxides have dielectric properties that are used in many microwave applications [5]. The high electrical resistivity of ferrites coupled with their low magnetic losses is critical in maintaining low insertion loss in microwave devices. Any electro-electronic device requests in its composition a permanent magnet. Barium Hexaferrite (BaFe₁₂O₁₉) has been used as a material that presents properties strongly related to the microstructure and morphology. The decrease in the size of the particle results in

advantages, such as high coercivity values, applicability in high frequency, low cost, great resistance to heat and high resistance to corrosion, in comparison to other materials that carry out the same function [6]. Barium Hexaferrite attracted many researchers to synthesis it by various techniques. Raghuram et al. [7] and Elbasuney et al. [8] synthesized $\text{BaFe}_{12}\text{O}_{19}$ by using a hydrothermal method. Moreover, sol-gel method [9-10], sonochemical approach [11], mechanically alloying method [12] and polymeric complex method (Pechini) [13] were previously reported for successful synthesis of $\text{BaFe}_{12}\text{O}_{19}$. However, in this study, co-precipitation method is used due to its simplicity, lower cost and flexibility [14]. Also, co-precipitation method controlled the size and the shape of the nanoparticles by adjusting the pH.

The present paper studies the effects of both Cobalt addition and calcination temperatures on the microstructure and the dielectric properties of barium Hexaferrite $\text{BaFe}_{12}\text{O}_{19}$. For that purpose, $\text{Co}_x\text{BaFe}_{12}\text{O}_{19}$ with $x = 0, 0.04, 0.06$ and 0.1 wt. % were synthesized by the co-precipitation method at different calcination temperatures (900°C and 950°C). Samples' microstructure characterization was performed through XRD and TEM techniques. The dielectric properties of the samples were studied using HIOKI 3532-50 LCR-Hi TESTER in frequency and temperature ranges of 100 kHz-3MHz and $25\text{-}500^\circ\text{C}$, respectively.

Experimental Technique

Synthesis by Co-precipitation Method

Barium Hexaferrite nanoparticles ($\text{BaFe}_{12}\text{O}_{19}$) added with x amount of Cobalt (Co), $0.00 \leq x$ (wt. %) ≤ 0.10 , were synthesized by co-precipitation method. An aqueous solution of Iron (III) chloride hexahydrate ($\text{FeCl}_3 \cdot 6\text{H}_2\text{O}$), Cobalt Chloride (CoCl_2) and Barium Chloride Dihydrate ($\text{BaCl}_2 \cdot 2\text{H}_2\text{O}$) was formed by dissolving these materials in suitable amounts of distilled water. Poly vinyl pyrrolidone (PVP) solution was prepared by dissolving 4g of this polymer in 100 mL distilled water and heated at 80°C for 15 minutes. The two aqueous solutions were mixed and kept under constant stirring by using a magnetic stirrer. Continuous addition of NaOH was done in a drop-wise manner until the pH became 13. The solution obtained was then maintained at a constant temperature of 60°C for

2 hours with constant stirring rate till $\text{Co}_x\text{BaFe}_{12}\text{O}_{19}$ nanoparticles were formed, which was visualized from the dark brown color of the mixture. After that, the mixture was left to cool down naturally for few minutes. The resultant brownish color product was washed continuously with distilled water in order to remove the residues, until the pH was 7 and then dried at 100°C for 18 hours in air. The dried ingots were then heated at different calcination temperatures (900°C and 950°C) for 2 hours.

Sample Characterization and Measurement

XRD patterns of $\text{Co}_x\text{BaFe}_{12}\text{O}_{19}$ were obtained by using Bruker D8 advanced power diffractometer with $20^\circ < 2\theta < 65^\circ$ range and Cu-K_α radiation ($\lambda = 1.54056 \text{ \AA}$). The surface morphology and particle size were examined using transmission electron microscopy (TEM) using Joel JEM-100Cx microscope at an accelerating voltage of 80 kV.

$\text{Co}_x\text{BaFe}_{12}\text{O}_{19}$ nanoparticles were pressed with a load of 13 tons and heated at 900°C and 950°C , the same as their calcination temperatures, for 2 hours. This process was carried out in order to provide more densification and less porosity, reducing the dielectric loss and allowing the storage of more energy. A very thin layer of silver paint was applied at the opposite surfaces of the formed pellets at room temperature. Silver paint was used because of its high conductivity and high melting point (i.e., above 500°C). Due to the low porosity formation and well compact pellets of investigated samples, there is a difficult possibility for diffusing the silver paint between the pore of compact samples. The coated pellet with silver paint was used in the HIOKI 3532-50 LCR HiTESTER in frequency and temperature ranges of 100 kHz-3MHz and 25°C - 500°C , respectively, where the parallel capacitance (C_p) and loss tangent ($\tan \delta$) were measured.

The following relations relate the real part of the dielectric constant (ϵ'), the imaginary part of the dielectric constant (ϵ'') and ac conductivity (σ_{ac}) to the parallel capacitance (C_p) and loss tangent ($\tan \delta$).

$$\epsilon' = \frac{C_p d}{\epsilon_0 A}, \quad (1)$$

$$\epsilon'' = \epsilon' \tan \delta, \quad (2)$$

$$\text{and } \sigma_{ac} = \epsilon_0 \omega \epsilon' \tan \delta, \quad (3)$$

where $\omega = 2 \pi f$ and f is the frequency of the applied ac field (Hz), d is the sample thickness ($d = 0.4$ cm), ϵ_0 is the permittivity of free space (8.85×10^{-12} F/m) and A is the area of the sample ($A = 5.3$ cm²).

Results and Discussion

Structural Analysis

Fig. 1 shows XRD patterns for Co_xBaFe₁₂O₁₉ nanoparticles, with $x = 0.00$ and 0.06 wt. %, prepared at calcination temperatures 900°C and 950°C . The observed peaks are well indexed by the hexagonal indices of BaFe₁₂O₁₉ (ICDD Card No-840757) with space group P63/mmc and in agreement with the Reitveld refinement shown in the inset of Fig. 1. These peaks correspond to the planes (006), (110), (112), (107), (114), (205), (206), (209), (004), (2011) and (220). Minor peak of α -Fe₂O₃ phase is also presented in the patterns indexed as (203) at $2\theta \approx 37^\circ$. Ding et al. [15] reported that, from Mössbauer spectra, α -Fe₂O₃ is usually associating the formation of

Barium Hexaferrite. The BaFe₁₂O₁₉ phase percentages are calculated and are listed in Table 1. It is clear that BaFe₁₂O₁₉ phase percentage is enhanced with increasing both the addition content x to 0.1 wt. % and the calcination temperature to 950°C . This means that increasing Co-addition and calcination temperature reduces the percentage of the secondary phases and increases the percentage of BaFe₁₂O₁₉ phase. This may be attributed to the interstitial diffusion of barium atoms into the cation vacancy of α -Fe₂O₃. Packiaraj et al. [16] reported similar results. They concluded that by increasing the calcination temperature, the intermediate phases, such as γ -Fe₂O₃, α -Fe₂O₃ and BaFe₂O₄, decreased whereas BaFe₁₂O₁₉ phase increased and appeared as a major phase at 950°C . Zhong et al. [17] reported about the fact that the appearance of α -Fe₂O₃ with orthorhombic hexahedron structure prevents the formation of BaFe₁₂O₁₉ hexagonal structure at low temperatures below 750°C .

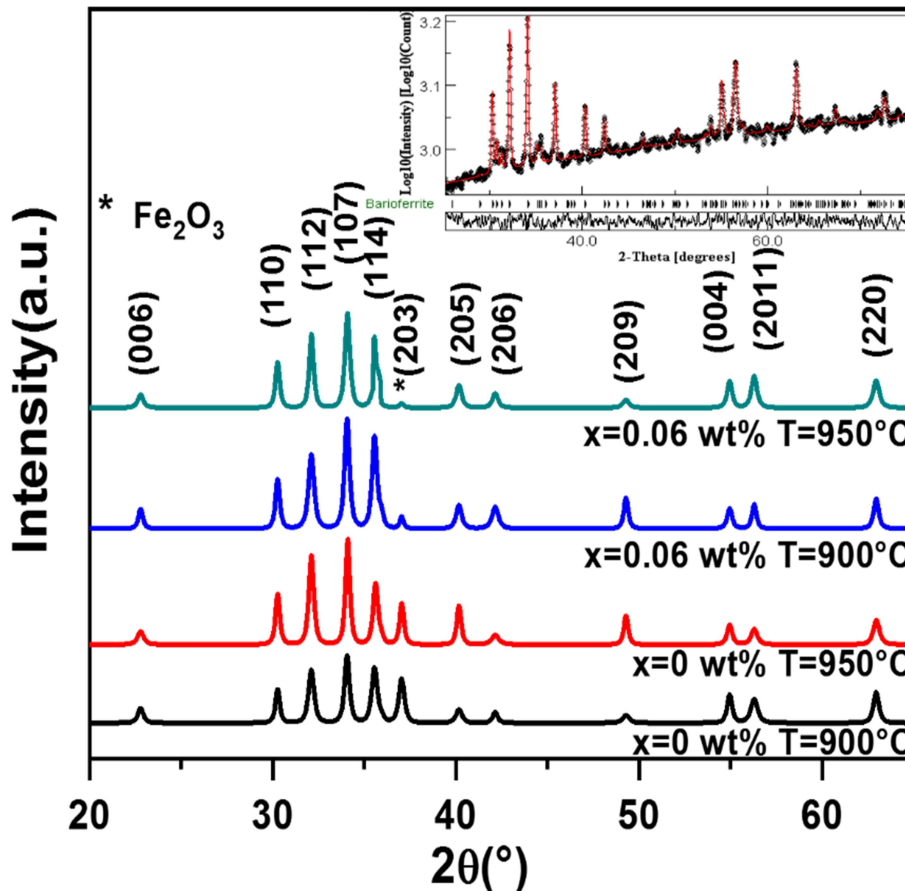


FIG. 1. XRD patterns for $x = 0.00$ and 0.06 wt. % at $T = 900^\circ\text{C}$ and 950°C with the inset of Reitveld refinement.

Lattice parameters (a and c) were calculated using MAUD program and unit cell volume V was calculated using equation $V = \frac{\sqrt{3}}{2} a^2 c$. The ratio c/a is constant for all prepared samples. The average crystallite size of the samples was calculated using Debye-Scherrer equation $D = \frac{S\lambda}{\beta_{hkl} \cos\theta}$, where D is the average crystallite size in nm, S is the shape factor which is equal to 0.9, λ is the wavelength of the X-ray radiation, β_{hkl} is the peak width at half-maximum intensity and θ is the peak position. The values of a, c, V and D at different calcination temperatures (T= 900°C and 950°C) for $\text{Co}_x\text{BaFe}_{12}\text{O}_{19}$ are listed in Table 1. As can be seen from Table 1, the values of a, c and V are slightly varied with either Cobalt addition or calcination temperatures. This indicates that Cobalt occupies only interstitial places in the Barium Hexaferrite matrix without entering the structure. Also, it is clear that the crystallite size D has unsystematic variation with

both x and T and that samples sintered at 950°C, except for x = 0.04 wt. % sample, have higher values of D in comparison with their counterparts sintered at 900°C. This result is consistent with the XRD peak width that becomes narrower with increasing calcination temperature to 950°C (see Fig. 1), which indicates that the average crystalline size of the prepared ferrites increased gradually. Kaur et al. [18] reported similar variations in crystallite size. The decrease in crystalline size may be attributed to smaller ionic radii of Co (0.625 Å) than Fe (0.63 Å) and Ba (1.11 Å), while the increase in crystalline size may be explained by cobalt ions being dissolved in $\text{BaFe}_{12}\text{O}_{19}$ grains and the excess of these ions being directed towards the grain boundaries, thus enhancing the liquid phase sintering. The value of c/a is almost constant and equal to 3.93, meaning that the crystal structure may be thought of as composed of planes of closely packed atoms.

TABLE 1. $\text{BaFe}_{12}\text{O}_{19}$ phase percentage, lattice parameters (a and c), unit cell volume (V), crystalline size (D) and grain size (D_{TEM}) of $\text{Co}_x\text{BaFe}_{12}\text{O}_{19}$ nanoparticles with ($0 \leq x \leq 0.10$) at calcination temperatures= 900°C and 950°C.

T (°C)	x (wt%)	$\text{BaFe}_{12}\text{O}_{19}$ (%)	a (Å)	c (Å)	c/a	V (Å ³)	D (nm)	D_{TEM} (nm)	I
900	0.00	90.36	5.87	23.14	3.93	692.6	51.5	80.29	1.55
	0.04	90.43	5.88	23.21	3.93	693.6	55.57	73.61	1.32
	0.06	90.83	5.87	23.16	3.94	696.9	51.42	74.56	1.45
	0.10	90.84	5.87	23.12	3.93	693.0	54.98	95.52	1.73
950	0.00	91.01	5.87	23.13	3.93	692.7	58.76	95.65	1.62
	0.04	91.02	5.87	23.13	3.93	693.3	52.02	69.82	1.34
	0.06	91.69	5.87	23.16	3.94	693.9	54.60	82.40	1.51
	0.10	91.72	5.87	23.12	3.93	692.0	57.54	164.51	2.85

TEM Investigation

The shape as well as the average particle size of pure and Cobalt-added $\text{Co}_x\text{BaFe}_{12}\text{O}_{19}$ nanoparticles were examined using TEM technique. Figs. 2a-d show TEM micrographs coupled with their Gaussian distribution of $\text{Co}_x\text{BaFe}_{12}\text{O}_{19}$ with x= 0.00 and x= 0.06 wt. %, at T = 900°C and T = 950°C, respectively. The average particle sizes D_{TEM} are calculated from the mean of the Gaussian distribution and are listed in Table 1. The average particle sizes for all the synthesized samples are in the range of 69-164 nm. Moreover, the particle sizes show nonlinear variation with Co-addition and increasing calcination temperature. This result is consistent with the behaviour of the average crystallite sizes D calculated from XRD analysis. It is clear from the micrographs that the samples

are mainly composed of agglomerated grains that form clusters of different sizes and shapes. In addition, it is clear that the sample morphology is changed to some extent to agglomerated hexagonal grains with increasing Co-addition and calcination temperature, as shown in Fig. 2d. Jurek et al. [19] observed hexagonal shaped particles for Barium Hexaferrite with diameter 50–70 nm. The crystallinity index (I) is investigated to check the crystallinity of the sample and is calculated by the following equation:

$$I = D_{\text{TEM}}/D_{\text{XRD}} \quad (4)$$

All the values obtained are listed in Table 1. They are found to be in the range of (1.32 -2.85). These values indicate that the samples are monocrystalline samples.

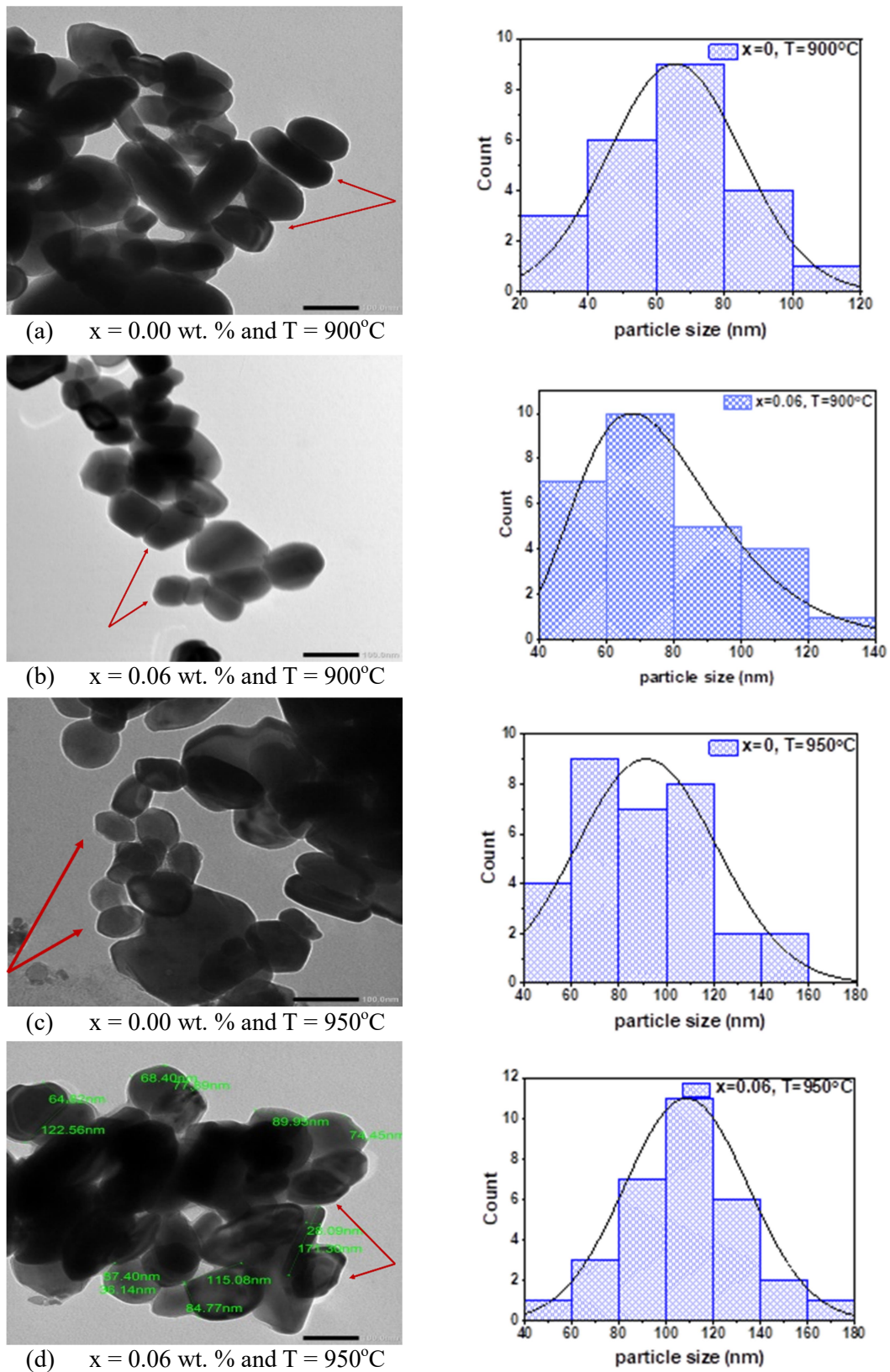


FIG. 2. TEM micrographs with 100 nm magnification scale and Gaussian distribution of $\text{Co}_x\text{BaFe}_{12}\text{O}_{19}$ with (a) $x = 0.00$ and at $T = 900^\circ\text{C}$, (b) $x = 0.06$ wt.% and at $T = 900^\circ\text{C}$, (c) $x = 0.00$ and at $T = 950^\circ\text{C}$ and (d) $x = 0.06$ wt.% and at $T = 950^\circ\text{C}$.

Dielectric Properties

Fig. 3(a) shows the variation of the real part of the dielectric constant (ϵ') with frequency (f) at fixed temperature $T=500^\circ\text{C}$ for $\text{Co}_x\text{BaFe}_{12}\text{O}_{19}$ (with $x = 0, 0.04, 0.06$ and 0.1 wt. %) samples calcined at 900°C and 950°C . The dielectric response can be visualized as; in the low frequency region (10^3 Hz) ϵ' has high values which decrease rapidly with increasing frequency followed by a plateau with lower values in the high frequency region (10^4 - 10^6 Hz). This behaviour can be explained on the basis of Koop's phenomenological theory and Maxwell Wagner theory [20]. This could be related to an electron hopping between Fe^{3+} and

Fe^{2+} ions. This will lead to the displacement of the ionic charges and is also responsible for interfacial polarization. Also, at low frequencies, the free charge carriers at grain boundaries or oxygen ion vacancies during the sintering process could have an effective contribution to interfacial polarization. Due to heat treatment, the structure of ferrite materials is supposed to be made of conducting grains separated by less conducting grain boundaries [21]. When hopping time is less than a half of the alternating field only, the electric field displaces the electrons, which leads to polarization. As a result, the dielectric constant will decrease at high frequency [22].

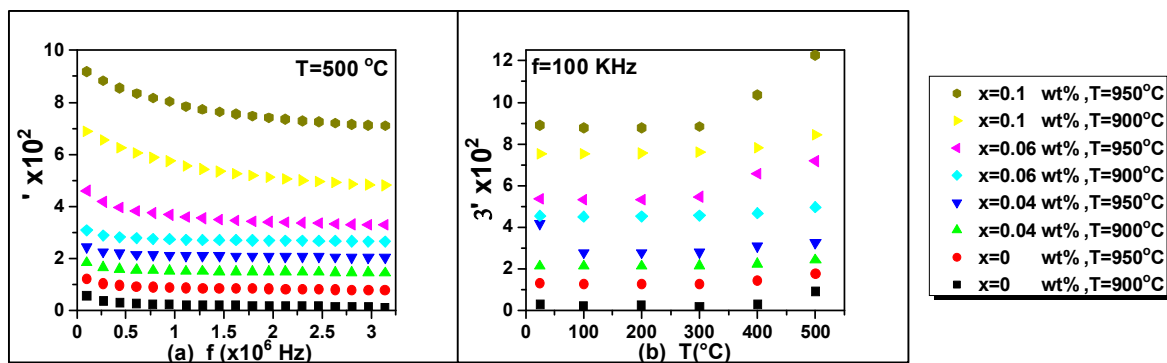


FIG. 3. The variation of ϵ' with (a) frequency at fixed temperature $T = 500^\circ\text{C}$ and (b) temperature at fixed frequency $f = 100$ kHz for $\text{Co}_x\text{BaFe}_{12}\text{O}_{19}$ calcined at 900°C and 950°C .

The variation of ϵ' with temperature at fixed frequency of 100 kHz for $\text{Co}_x\text{BaFe}_{12}\text{O}_{19}$ samples is shown in Fig. 3(b). It can be seen that ϵ' values show increment with increasing temperature from 25°C to 500°C . Finally, it is noted that ϵ' is strongly dependent on both Co-addition and calcination temperature, as it increases with increasing Co-addition from 0 to 0.1 wt. % and samples sintered at 950°C have higher values of ϵ' than those sintered at 900°C .

Fig. 4(a) displays the variation of the imaginary part of the dielectric constant (ϵ'') with frequency (f) at fixed temperature $T = 500^\circ\text{C}$ for $\text{Co}_x\text{BaFe}_{12}\text{O}_{19}$ (with $x = 0, 0.04, 0.06$ and 0.1 wt. %) samples calcined at 900°C and 950°C . It is clearly observed from Fig. 4(a) that the variation behavior of ϵ'' with frequency is very similar to the variation of ϵ' with f . Similarly, ϵ'' is found to exhibit a sharp decrease in the low-frequency region, then as the frequency increases, ϵ'' is observed to decrease slowly until it becomes independent on frequency at high-frequency range. The high values of ϵ'' obtained for all samples at low

frequency can be also attributed to the microstructure characteristics and morphological parameters, such as density, porosity, grain boundary sizes and other crystalline defects [23, 24], which results in space-charge polarization increment and consequently enhancement in the values of ϵ'' . However, further decrease in ϵ'' values with the increase in frequency is explained by the idea that any species contributing to polarization is found to show lagging behind the applied field as frequency becomes higher and higher.

Fig. 4(b) displays the variation of the imaginary part of the dielectric constant ϵ'' with temperature at fixed frequency $f = 100$ kHz. It is clearly observed from the figure that ϵ'' increases with increasing temperature. This result can be explained by dipolar and interfacial polarizations, but it is more noticeable in the interfacial polarization, where hoping of more electrons takes place under the thermal effect. This result was confirmed by Maxwell Wagner model [25].

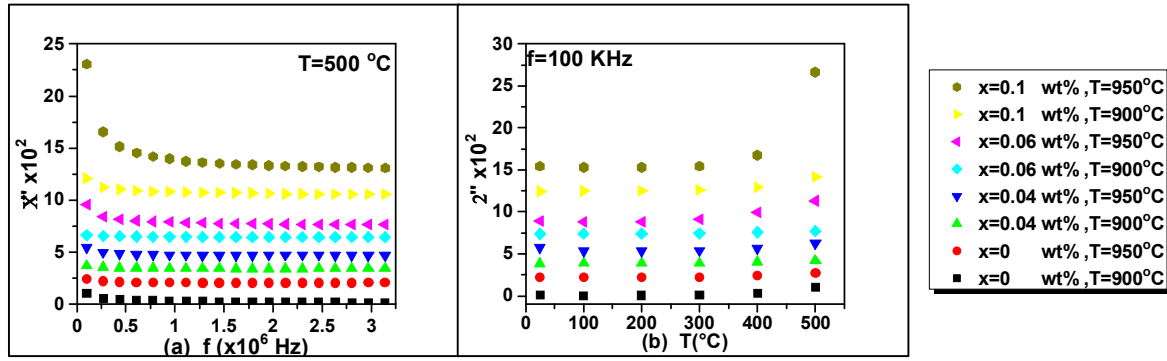


FIG. 4. The variation of ϵ'' with (a) frequency at fixed temperature $T = 500^\circ\text{C}$ and (b) temperature at fixed frequency $f = 100\text{ kHz}$ for $\text{Co}_x\text{BaFe}_{12}\text{O}_{19}$ calcined at 900°C and 950°C .

The behavior of dielectric loss ($\tan \delta$) with frequency at fixed temperature $T = 500^\circ\text{C}$ for $\text{Co}_x\text{BaFe}_{12}\text{O}_{19}$ (with $x = 0, 0.04, 0.06$ and 0.1 wt. %) samples calcined at 900°C and 950°C is shown in Fig. 5(a). It is clear that after reaching a maximum value, dielectric loss $\tan \delta$ decreases with increasing frequency. The high dielectric constant is a result of hopping, where the loss tangent behavior can similarly be explained on this basis. When the hopping is nearly equal to that of the externally applied electric field, maximum of loss tangent could be observed.

After reaching the maximum, hopping time becomes more than the applied signal, which causes a decrease in loss tangent.

The dielectric loss ($\tan \delta$) as a function of temperature is represented in Fig. 5(b), where the dielectric loss ($\tan \delta$) increases with increasing calcination temperature. The dipole orientation increases as the temperature increases and as a result, the dipole losses increase. This means that more electrons and space charge polarizations were manifesting at higher temperatures [25].

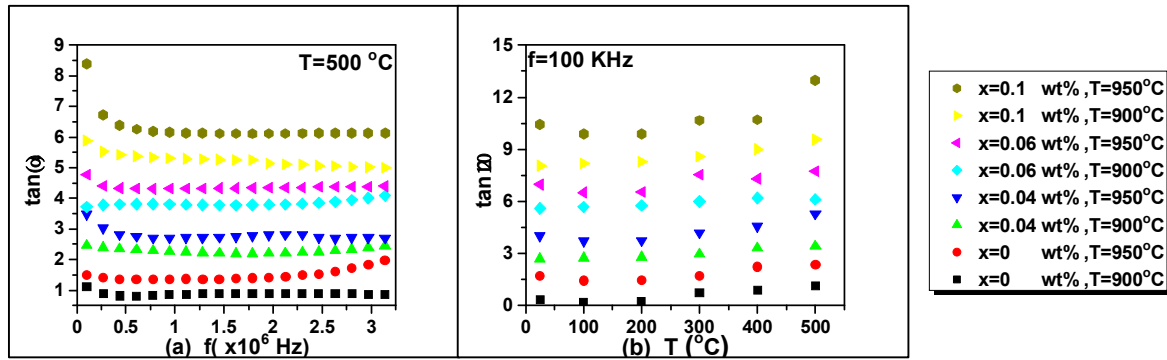


FIG. 5. The variation of $\tan \delta$ with (a) frequency at fixed temperature $T = 500^\circ\text{C}$ and (b) temperature at fixed frequency $f = 100\text{ kHz}$ for $\text{Co}_x\text{BaFe}_{12}\text{O}_{19}$ calcined at 900°C and 950°C .

The ac conductivity (σ_{ac}) dependence on frequency at fixed temperature $T = 500^\circ\text{C}$ for $\text{Co}_x\text{BaFe}_{12}\text{O}_{19}$ (with $x = 0, 0.04, 0.06$ and 0.1 wt. %) samples calcined at 900°C and 950°C is recorded in Fig. 6(a). The results show that σ_{ac} exhibits an increasing trend with the increase in the applied ac field frequency. The increase in conductivity is due to the increase in the charge carriers as the applied frequency increases [26]. Similar increasing trends were reported for several ferrites [27-28]. At lower frequencies, the poor-conducting grain boundaries are active and hence the exchange between Fe^{2+} and Fe^{3+}

ions is low and this explains the low values of σ_{ac} obtained at low frequency. However, as the frequency increases, the conductive grains become more active than the grain boundaries causing an increase in the exchange between Fe^{2+} and Fe^{3+} ions and therefore an increase in the conduction [20] and consequently in the σ_{ac} values. It is clear from Fig. 6(b) of σ_{ac} versus temperature at $f = 100\text{ kHz}$ that the temperature greatly affects the ac conductivity, σ_{ac} . At high temperature, the charge carriers are thermally activated; so their velocity increases, leading to an increase in conductivity.

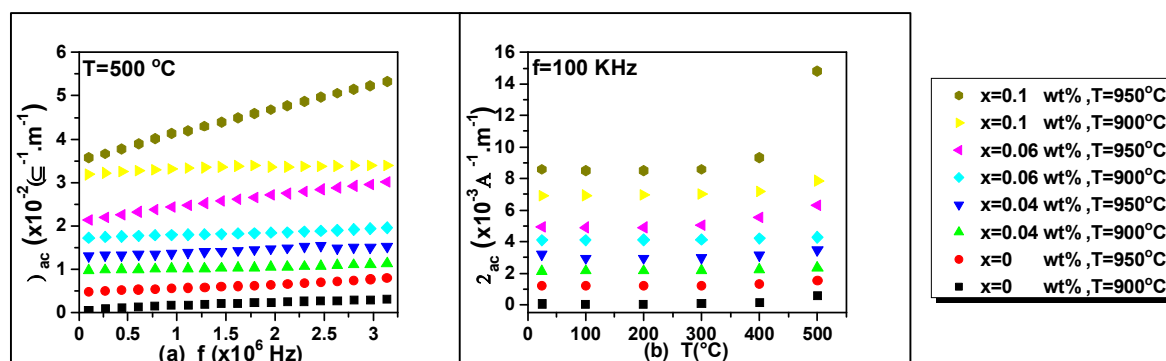


FIG. 6. The variation of σ_{ac} with (a) frequency at fixed temperature $T = 500^\circ\text{C}$ and (b) temperature at fixed frequency $f = 100 \text{ kHz}$ for $\text{Co}_x\text{BaFe}_{12}\text{O}_{19}$ calcined at 900°C and 950°C .

Conclusion

Chemical co-precipitation method was successfully utilized to prepare nanoparticles of $\text{Co}_x\text{BaFe}_{12}\text{O}_{19}$, with $x = 0, 0.04, 0.06$ and $0.1 \text{ wt. } \%$. The effects of Cobalt addition and calcination temperature (900°C and 950°C) on the microstructure, morphology and dielectric properties of the synthesized samples were investigated. XRD results revealed the hexagonal structure of the prepared samples and indicated enhancement in the phase formation of $\text{BaFe}_{12}\text{O}_{19}$ and reduction of Fe_2O_3 phase with increasing both the Co-addition and calcination temperature. Moreover, the lattice parameters (a and c) and unit cell volume (V) were almost unchanged with either Cobalt addition or calcination temperatures. By the use of Debye–Scherrer equation, the crystallite size was varied from $51\text{--}58 \text{ nm}$. Samples morphology was studied through TEM technique. TEM micrographs clarified that the samples are mainly composed of agglomerated grains that form hexagonal-shaped particles. The behaviours of the dielectric constants (ϵ' and ϵ''), loss tangent ($\tan \delta$) and ac conductivity (σ_{ac}) have

been explained on the basis of hopping of electrons between Fe^{2+} and Fe^{3+} ions. Moreover, the Co-addition and the calcination temperature elevation lead to higher dielectric constants (11.9×10^2 at $T=500^\circ\text{C}$ and $f=100 \text{ kHz}$) and enhanced ac conductivities ($15.1 \times 10^{-3} \text{ A}^{-1}\text{m}^{-1}$) for samples calcined at 950°C . As a conclusion, the dielectric properties are highly dependent on the hexagonal structure of the $\text{Co}_x\text{BaFe}_{12}\text{O}_{19}$ and the exchange between $\text{Fe}^{2+}\text{--}\text{Fe}^{3+}$ ions. In addition, it is noted that as the calcination temperature increases, the crystallite size increases with an enhancement in both real and imaginary dielectric constants, $\tan \delta$ and ac conductivity.

Acknowledgement

This work was performed in the materials science lab, Physics Department, Faculty of Science, Beirut Arab University, Beirut, Lebanon; in cooperation with Physics Department, Alexandria University, Alexandria, Egypt and Physics Department, Lebanese University, Beirut, Lebanon.

References

- [1] Kaur, T., Kaur, B., Bhat, B.H., Kumar, S. and Srivastava, A.K., *Physica B: Condensed Matter*, 456 (2015) 206.
- [2] Martirosyan, K.S., Galstyan, E., Hossain, S.M., Wang, Y.J. and Litvinov, D., *Mater. Sci. Eng. B*, 176 (2011) 8.
- [3] Pullar, R.C., *Prog. Mater. Sci.*, 57 (2012) 1191.
- [4] Rashad, M.M. and Ibarhim, I.A., *J. Supercond. Nov. Magn.*, 26 (2013) 1639.
- [5] Mallick, K.K., Shepherd, P. and Green, R.J., *Journal of the European Ceramic Society*, 27 (2007) 2045.
- [6] Pereira, F.M.M., Santos, M.R.P., Sohn, R.S.T.M., Almeida, J.S., Medeiros, A.M.L., Costa, M.M. and Sombra, A.S.B., *Journal of Materials Science: Materials in Electronics*, 20 (2009) 408.
- [7] Raghuram, N., Rao, T.S. and Babu Naidu, K.C., *Materials Science in Semiconductor Processing*, 94 (2019) 136.

- [8] Elbasuney, S., Gobara, M. and Yehia, M., *Journal of Inorganic and Organometallic Polymers and Materials*, 29 (2019) 721.
- [9] Almessiere, M.A., Slimani, Y., Tashkandi, N.A., Baykal, A., Saraç, M.F., Trukhanov, A.V., ... and Özçelik, B., *Ceramics International*, 45 (2019) 1691.
- [10] Zhuravlev, V.A., Itin, V.I., Minin, R.V., Lopushnyak, Y.M., Svetlichnyi, V.A., Lapin, I.N., ... and Lilenko, I.Y., *Journal of Alloys and Compounds*, 771 (2019) 686.
- [11] Sadaqat, A., Almessiere, M., Slimani, Y., Guner, S., Sertkol, M., Albetran, H., ... and Ercan, I., *Ceramics International*, 45 (2019) 22538.
- [12] Manafi, S.A., Jougehdoost, S., Kiahosseini, S.R. and Farahbakhsh, I., *Journal of the Australian Ceramic Society*, 55 (2019) 371.
- [13] Urbano-Peña, M.A., Palomares-Sánchez, S.A., Betancourt, I., Pérez-Juache, T.J. and Ruiz, F., *Applied Physics A*, 125 (2019) 711.
- [14] Hu, S.L., Liu, J., Yu, H.Y. and Liu, Z.W., *Journal of Magnetism and Magnetic Materials*, 473 (2019) 79.
- [15] Ding, J., Yang, H., Miao, W.F., McCormick, P.G. and Street, R., *Journal of Alloys and Compounds*, 221 (1995) 70.
- [16] Packiaraj, G., Panchal, N. and Jotania, R.B. *International Journal of Systems Biology*, 2 (2010) 5.
- [17] Zhong, W., Ding, W., Jiang, Y., Zhang, N., Zhang, J., Du, Y. and Yan, Q., *Journal of the American Ceramic Society*, 80 (1997) 3258.
- [18] Qiu, J., Zhang, Q., Gu, M. and Shen, H., *Journal of Applied Physics*, 98 (2005) 103905.
- [19] Ziełńska-Jurek, A., Bielan, Z., Dudziak, S., Wolak, I., Sobczak, Z., Klimczuk, T. and Hupka, J., *Catalysts*, 7 (2017) 360.
- [20] Singh, A., Narang, S.B., Singh, K., Pandey, O.P. and Kotnala, R.K., *J. Ceram. Process. Res.*, 11 (2010) 241.
- [21] Ali, I., Islam, M.U., Awan, M.S. and Ahmad, M., *J. Electron. Mater.*, 43 (2014) 512.
- [22] Narang, S.B. and Hudhara, I.S., *J. Ceram. Process. Res.*, 7 (2006) 113.
- [23] Ali, I., Islam, M.U., Awan, M.S. and Ahmad, M., *J. Mater. Eng. Perform.*, 22 (2013) 2104.
- [24] Hajalilou, A., Kamari, H.M. and Shameli, K., *Journal of Alloys and Compounds*, 708 (2017) 813.
- [25] Mansour, S.F. and Abdo, M.A., *Journal of Magnetism and Magnetic Materials*, 428 (2017) 300.
- [26] Hankare, P.P., Sankpal, U.B., Patil, R.P., Jadhav, A.V., Garadkar, K.M. and Chougule, B.K., *Journal of Magnetism and Magnetic Materials*, 323 (2011) 389.
- [27] Melagiriappa, E., Jayanna, H.S. and Chougule, B.K., *Materials Chemistry and Physics*, 112 (2008) 68.
- [28] El-Ata, A.A., El-Nimr, M.K., Attia, S.M., El-Kony, D. and Al-Hammadi, A.H., *Journal of Magnetism and Magnetic Materials*, 297 (2006) 33.